

## Precise smart model for estimating dynamic viscosity of SiO<sub>2</sub>/ethylene glycol–water nanofluid

Mohammad Hossein Ahmadi, Milad Sadeghzadeh, Heydar Maddah, Alireza Solouk, Ravinder Kumar & Kwok-wing Chau

To cite this article: Mohammad Hossein Ahmadi, Milad Sadeghzadeh, Heydar Maddah, Alireza Solouk, Ravinder Kumar & Kwok-wing Chau (2019) Precise smart model for estimating dynamic viscosity of SiO<sub>2</sub>/ethylene glycol–water nanofluid, Engineering Applications of Computational Fluid Mechanics, 13:1, 1095-1105, DOI: [10.1080/19942060.2019.1668303](https://doi.org/10.1080/19942060.2019.1668303)

To link to this article: <https://doi.org/10.1080/19942060.2019.1668303>



© 2019 The Author(s). Published by Informa UK Limited, trading as Taylor & Francis Group.



Published online: 01 Oct 2019.



Submit your article to this journal [↗](#)



Article views: 120



View related articles [↗](#)



View Crossmark data [↗](#)

## Precise smart model for estimating dynamic viscosity of SiO<sub>2</sub>/ethylene glycol–water nanofluid

Mohammad Hossein Ahmadi<sup>a</sup>, Milad Sadeghzadeh<sup>b</sup>, Heydar Maddah<sup>c</sup>, Alireza Solouk<sup>b</sup>, Ravinder Kumar<sup>d</sup> and Kwok-wing Chau<sup>e</sup>

<sup>a</sup>Faculty of Mechanical Engineering, Shahrood University of Technology, Shahrood, Iran; <sup>b</sup>Department of Renewable Energy and Environmental Engineering, University of Tehran, Tehran, Iran; <sup>c</sup>Department of Chemistry, Payame Noor University (PNU), Tehran, Iran; <sup>d</sup>School of Mechanical Engineering, Lovely Professional University, Punjab, India; <sup>e</sup>Department of Civil and Environmental Engineering, Hong Kong Polytechnic University, Hong Kong, People's Republic of China

### ABSTRACT

Artificial neural network (ANN) is widely being used in engineering applications in order to provide predicting models to estimate the performance of the studied system under specific working conditions. One of the significant characteristics that are highly practical in fluid mechanics and heat transfer systems is the dynamic viscosity which highly affects pressure drop and also has an influence on the heat transfer performance. Due to the lack of a precise model to predict the dynamic viscosity, in this research, experimentally measured dynamic viscosity of SiO<sub>2</sub>/ethylene glycol–water nanofluid data is collected from the literature and used to present a smart model based on the ANN technique. In order to provide a precise smart model, Multilayer Perceptron (MLP) and Radial Basis Function (RBF) algorithms are applied in the neural network. The accuracy of the proposed model is validated through performing error analysis. It is monitored that the employed approach is highly potent in estimating high accuracy responses since the results of mean square and correlation coefficient analyses are 5.5 and 0.998 Pa s.

### ARTICLE HISTORY

Received 9 May 2019  
Accepted 11 September 2019

### KEYWORDS

Silicon oxide nanofluid;  
dynamic viscosity;  
nanoparticle diameter;  
artificial neural network

## 1. Introduction

Nanofluids are formed by adding nano-sized particles (1–100 nm) into conventional working fluids such as water, ethylene glycol, propylene glycol, glycol, and engine oil (Ahmadi, Sadeghzadeh, Raffiee, & Chau, 2019; Maddah et al., 2018; Mahyari, Karimipour, & Afrand, 2019). Insertion of nano-sized materials into the base fluid could significantly amend thermal characteristics such as thermal conductivity and also improve the heat transfer rate (Ahmadi et al., 2018; Kahani, Ahmadi, Tatar, & Sadeghzadeh, 2018). Wide variety of organic and inorganic nano-sized materials are employed in the preparation of nanofluids (Ramezanizadeh, Alhuyi Nazari, Ahmadi, & Açikkalp, 2018). These materials can be classified into metals such as Ag, Al, and Fe (Alawi, Sidik, Xian, Kean, & Kazi, 2018; Ghalandari, Mirzadeh Koohshahi, Mohamadian, Shamsheerband, & Chau, 2019), ceramics including Al<sub>2</sub>O<sub>3</sub>, CuO, Fe<sub>3</sub>O<sub>4</sub>, SiO<sub>2</sub>, and TiO<sub>2</sub>, and the group of inorganics such as graphene, single-walled carbon nanotubes (SWCNTs) or multi-walled carbon nanotubes (MWCNTs) (Cardellini, Fasano, Bozorg Bigdeli, Chiavazzo, & Asinari, 2016; Ghasemi & Karimipour, 2018; Moldoveanu,

Humnic, Minea, & Humnic, 2018). Interesting features of nanofluids have attracted and created an opportunity for researchers in several fields of engineering to probe physical specifications of these materials such as thermal conductivity and dynamic viscosity (Azari, Kalbasi, Derakhshandeh, & Rahimi, 2013; Nazari, Ahmadi, Sadeghzadeh, Shafii, & Goodarzi, 2019; Ramezanizadeh, Alhuyi Nazari, Ahmadi, & Chau, 2019; Sahoo, Das, Vajjha, & Satti, 2013). Ceramics such as silica nanoparticles demonstrated suitable stability, appropriate inertia to chemical reactions, lower density, lower electrical and thermal conductivities in comparison to metallic nanoparticles (Dalkılıç et al., 2018; Hamid, Azmi, Nabil, Mamat, & Sharma, 2018). In order to address wear resistance and stability in high temperatures, considerably silica nanoparticles could be employed as a substitute for metallic nanoparticles. While numerous investigations analyzed the thermal conductivity of metallic oxides such as Al<sub>2</sub>O<sub>3</sub> (Gupta, Singh, Kumar, & Said, 2017), a few just focused on assessing the impact of applying silica nanoparticles on the thermal conductivity and the dynamic viscosity of the nanofluid. Bobbo et al. (Bobbo et al., 2011) measured the thermal conductivity of SiO<sub>2</sub> in

**CONTACT** Mohammad Hossein Ahmadi  mhosein.ahmadi@shahroodut.ac.ir; Ravinder Kumar  rav.chauhan@yahoo.co.in

© 2019 The Author(s). Published by Informa UK Limited, trading as Taylor & Francis Group.  
This is an Open Access article distributed under the terms of the Creative Commons Attribution License (<http://creativecommons.org/licenses/by/4.0/>), which permits unrestricted use, distribution, and reproduction in any medium, provided the original work is properly cited.

water as the base fluid. Escher et al. (Escher et al., 2011) fabricated high concentrations of SiO<sub>2</sub>/water nanofluid and measured the thermal conductivity. It was monitored that there was no considerable difference between the measurements and the values of thermal conductivity which were obtained through the effective medium theory (EMT). In contrary, Peñas et al. (Peñas, de Zárata, & Khayet, 2008) monitored a deviation between the measured values and the EMT outputs. Abdolbaqi et al. (Abdolbaqi et al., 2016) stated that thermal conductivity was affected by the concentration of the nanofluid, nature of the base fluid, and also its temperature. Talib et al. (Talib et al., 2015) approved the impact of base fluid and concentration on the thermal conductivity. The authors experimented SiO<sub>2</sub>/ethylene glycol/water in different concentrations (0.1–0.5%). Kulkarni et al. (Kulkarni, Namburu, Bargar, & Das, 2008) carried out an experiment to determine the influence of applying SiO<sub>2</sub> nanoparticles at the various size (20, 50, and 100 nm) in a fluid consisted of water–ethylene glycol (40:60). It was monitored that increasing the size of the nanoparticles boosted up the heat transfer performance. It was also expressed that increasing the concentration of nanoparticles caused to increase the value of the pressure drop. Azmi et al. (Azmi et al., 2013) carried out an experimental investigation to analyze the effect of applying SiO<sub>2</sub>/water nanofluid in a circular tube. In the experiment, the volume concentration of the nanofluid was varied in the range of 0–4%, the average particle size was 22 nm, Re number in the range of 5000–27,000, 30°C as the bulk temperature, and boundary condition of constant heat flux were considered. It was found out from the results that increasing the volume concentration was yielded to increase the heat transfer coefficient up to 3% and more than this concentration the heat transfer coefficient followed a decreasing trend.

Various computational methods are employed in engineering applications to bring about targeted objectives such as predicting the output, behavior or a specific feature (Chuntian & Chau, 2002; Fotovatikhah et al., 2018; Taherei Ghazvinei et al., 2018). Artificial Neural Network (ANN) is one of this methods which is widely applied in engineering application specifically for the purpose of predicting or estimating (Ahmadi, 2015; Ahmadi & Mahmoudi, 2016; Chau, 2017; Hajikhodaverdikhan, Nazari, Mohsenizadeh, Shamshirband, & Chau, 2018; Wu & Chau, 2011). Razavi et al. (Razavi et al., 2019) studied the ability of ANFIS and LSSVM in predicting the effect of metal-based and metal-oxides nanofluids on the thermal performance. Amani et al. (Amani, Amani, Jumholkul, Mahian, & Wongwises, 2018) employed ANN structures and genetic algorithms to propose a correlation for estimating the pressure drop

and the Nusselt number of a flow while SiO<sub>2</sub> nanoparticles were applied. Sadeghzadeh et al. (Sadeghzadeh et al., 2019) used machine learning methods to evaluate the impact of using nanofluids in solar thermal collectors. Ramezanizadeh et al. (Ramezanizadeh, Alhuyi Nazari, Ahmadi, Lorenzini, & Pop, 2019) performed a review study and discussed the application of intelligent approaches in estimating thermal conductivity of nanofluids. In another study, Ramezanizadeh et al. (Ramezanizadeh, Ahmadi, Ahmadi, & Alhuyi Nazari, 2019) evaluated various intelligent techniques to propose a model to forecast the dynamic viscosity of Al<sub>2</sub>O<sub>3</sub>–water. Ahmadi et al. (Ahmadi, Mohseni-Gharyehsafa, et al., 2019) used several connectionist techniques to estimate dynamic viscosity of Ag nanoparticles in water. Sepehr et al. (Sepehr, Baghban, Ghanbari, Bozorgvar, & Baghban, 2018) employed LSSVM method to predict the dynamic viscosity of *n*-alkanes. Zhao et al. (Zhao, Wen, Yang, Li, & Wang, 2015) investigated the potential of radial basis function neural networks (RBF) method in estimating viscosity of water-based nanofluids, i.e. Al<sub>2</sub>O<sub>3</sub>–water and CuO–water. Baghban et al. (Baghban et al., 2019) performed an investigation to evaluate heat transfer performance of SiO<sub>2</sub>–water nanofluid in a quadrangular-shaped cross section. The authors assessed convective heat transfer coefficient under certain operational conditions of Re, Pr, and concentration of the nanoparticles. The experimental outputs then were introduced to various machine learning approaches including LSSVM, ANFIS, and PSO to present an accurate model which had this ability to predict the heat transfer behavior of the flow containing nanofluid at specified conditions.

In this study, a previously published database is used to estimate the dynamic viscosity of a nanofluid which is SiO<sub>2</sub>/ethylene glycol–water by applying ANN techniques (Kulkarni et al., 2008; Namburu, Kulkarni, Dandekar, & Das, 2007). The Dynamic viscosity is selected since it is an important parameter in fluid dynamic and heat transfer processes. ANN techniques have this potential to provide a numerical model with high precision output in order to save time and costs of real experiments. Multilayer perceptron (MLP) and RBF approaches were selected and applied to the gathered experimental data. Error analysis has been performed to demonstrate the accuracy of the presented model outputs.

## 2. Methodology

Several smart methods have been applied for predicting the thermal specifications of nanofluids so far. Among them, MLP and RBF are illustrated to be the most typical and also practical approach. The positive side of applying RBF network is the much robustness while the MLP

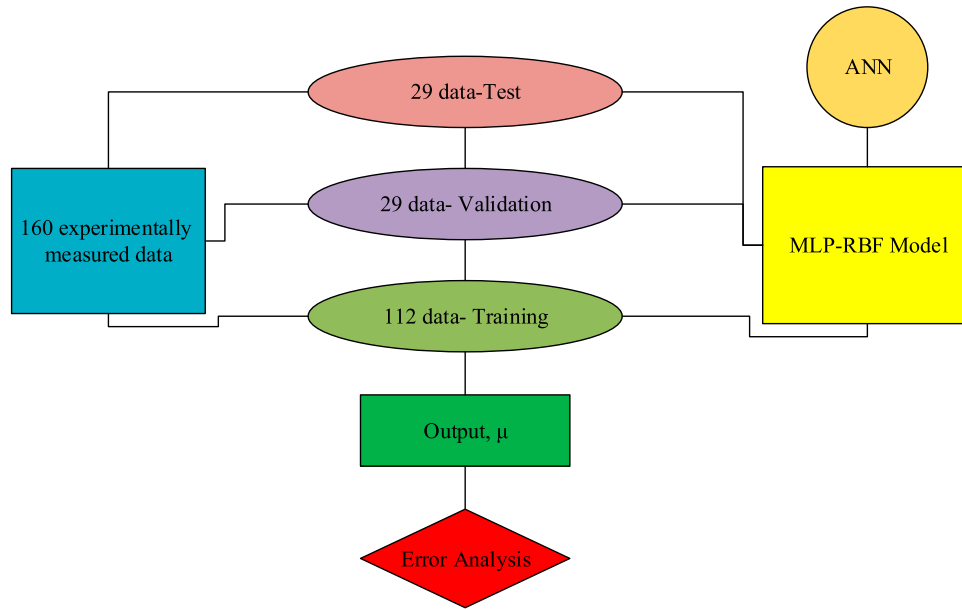


**Figure 1.** Schematic description of the study procedure.

showed a weakness to adversarial noise. In general, the comparative assessment between more precise results in MLP and higher robustness determines the selection of MLP or RBF technique.

The applied methodology is depicted in Figure 1. Based on this figure, the 160 collected data from the literature (Kulkarni et al., 2008; Namburu et al., 2007) was introduced to an ANN model, MLP and RBF, and then the outputs of the model were assessed through error analysis. 160 data were extracted from the following references. Moreover, 24 data was employed in the test stage, 24 data was applied in the validation stage, and other remaining 112 was utilized in the training stage. The input variables of this study are Concentration ratio, particle size and temperature. The output function of this study is viscosity. The proposed model fundamental is briefly discussed in the following figure.

### 2.1. MLP artificial neural network

MLP is an ANN approach which is vastly employed in optimization purposes (Zendehboudi, Wang, & Li, 2017). The schematic illustration of the MLP-ANN approach is presented in Figure 2.

Based on Figure 2, the MLP method comprises different nodes which are categorized into three layers: the input data are inserted into the first layer which is known as the input layer, a middle layers which are named as hidden layers, and the output layer illustrating the final estimation resulted out of the network. Each node has its own specific weight vector in order to form a connection with the nodes which are placed in the following layer.

In MLP-ANN, each node has this potential to act as the receiver, processor, and provider of the output response. The input layer' nodes are totally summed up and delivered as an input of the hidden layer (Zendehboudi & Li, 2017). Considering  $X$  as the input vector of the MLP approach:  $X = [x_1, x_2, x_3, \dots, x_n]^T$ , then,  $n_j$  expressed the hidden layer input associating to the  $j$ th node:

$$n_j = \sum_{i=1}^n \omega_{ji}x_i + \theta_j \quad j = 1, 2, \dots, K, \quad (1)$$

where  $\omega_{ji}$  is the inter-connections weight of  $j$ th node in the hidden layer and the  $i$ th node in the input layer,  $\theta$  represents the threshold of the  $j$ th node in the hidden layer, and  $K$  indicates the number of nodes in the hidden layer. In order to supply the total input of the hidden nodes in the hidden layer, utilization of a transfer function,  $f$ , is necessary:

$$y_j = f(n_j) = f\left(\sum_{i=1}^n \omega_{ji}x_i + \theta_j\right) \quad j = 1, 2, \dots, K. \quad (2)$$

Transfer functions are characterized and can be employed for different applications. The output of each node in the hidden layer is multiplied by its corresponding output weight connector. While the number of variables is the defining function in determining the number of neurons in the input and output layers of the MLP model, there is no approved method for specifying the size or the numbers of neurons in the hidden layers. The complexity of the model, amount of training data, amount of test data, and also the existed noise in the

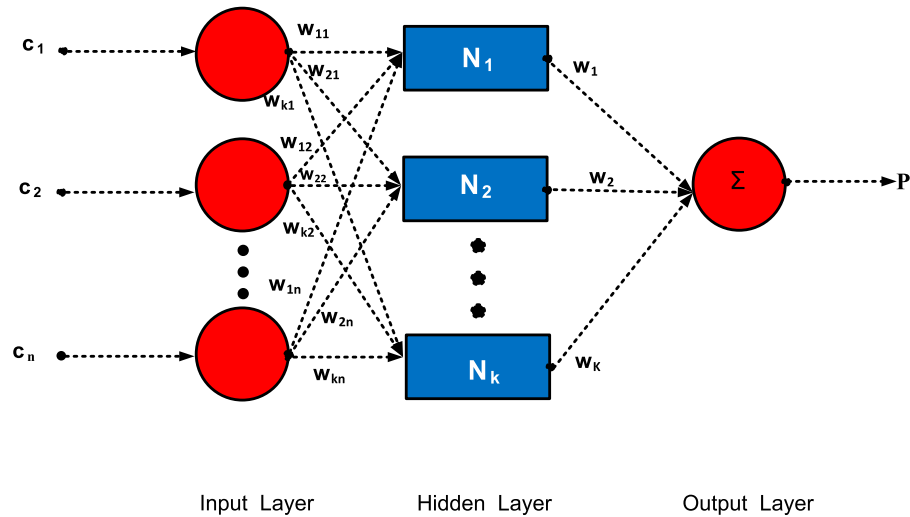


**Figure 2.** Schematic illustration of the MLP-ANN method (Zendeboudi et al., 2017).

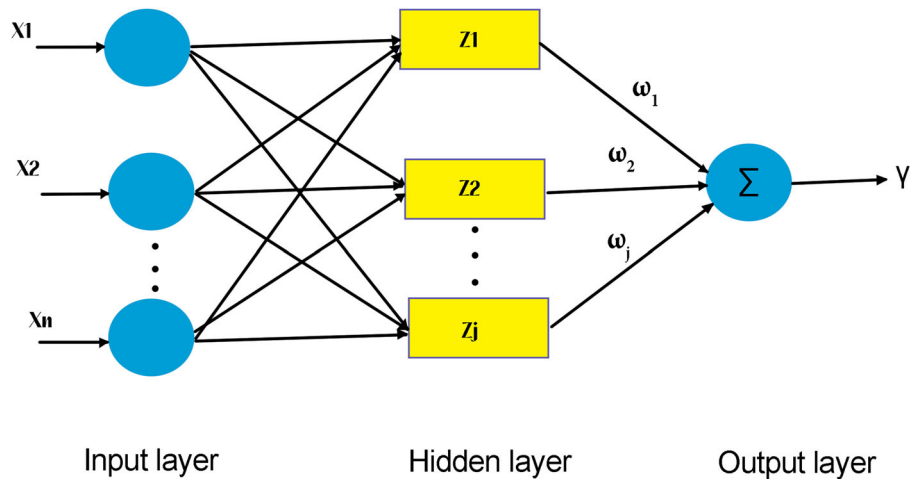


**Figure 3.** A typical RBF layout (Zendeboudi & Tatar, 2017).

employed data are the affecting factor in determining the number of hidden layers (Du & Swamy, 2006). Therefore, neurons are continuously added to the hidden layer to obtain the optimum amount of neurons based on an iteration procedure. Presence of a training stage is vital in the formation of an estimating MLP model. The estimating procedure is happened by setting the weight and biases according to the data sets of input and output. The MLP model requires a training phase and to address this issue Backpropagation (BP) algorithm is employed to set the weights and biases (Goh, 1995).

## 2.2. RBF network

The RBF neural network has some advantages over other approaches. These advantages are its direct layout, exact precision, and also fast training phase. The RBF network is an effective feed-forward neural network layout. Figure 3 demonstrates a typical structure of the RBF method.

The RBF algorithm is comprised of an input layer, a hidden layer, and an output layer. Every node in different layers is thoroughly connected to the previous layer of the algorithm. The input data is inserted to the input layer and a node is assigned to each data and then directly transferred into the hidden layer. In the last stage, weighted links are employed to deliver data to the output layer. In the RBF approach, the momentous stage is the hidden layer. In the hidden layer, the RBF is performed as the activation function to generate the distance vector multiplied by the corresponding bias. The hidden layer is charged to plan the input vectors to a new space (Zendeboudi & Tatar, 2017). The hidden layer produces the  $j$ th neuron as the output which is obtained as follows:

$$Z_j = Z(\|X - \Delta_j\|) = \exp\left(-\frac{\|X - \Delta_j\|^2}{2\xi_j^2}\right), \quad (3)$$

where  $Z$  states the RBF function which is here the Gaussian function,  $X$  indicates the input vector,  $\Delta_j$

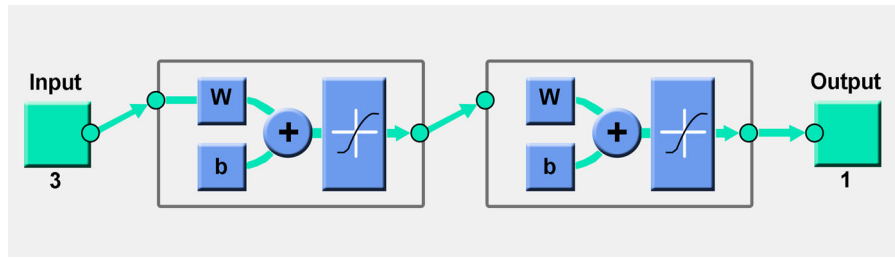


**Figure 4.** A three layer NN model with an arrangement of 3–7–1–1 to estimate the viscosity of nanofluid.

expresses the weight factor, and  $\xi_j$  denotes the standard deviation. The symbol of  $\| \cdot \|$  expresses the Euclidean norm. The standard deviation is calculated as

$$\xi = \frac{\theta_m}{\sqrt{\Lambda}}, \quad (4)$$

where  $\theta_m$  indicates the largest center-to-center distance.  $\Lambda$  denotes the number of centers. At last, the weighted sum of the signals from the hidden layer transferred and gathered into the output layer:

$$\gamma = \sum_{j=1}^A \omega_j Z_j, \quad (5)$$

where  $\omega_j$  represents the weight vectors and it is obtained through the training stage.

### 3. ANN modeling structure

Neural Network (NN) is a data-guided model. Therefore, experimental data is required to build the model. In this study, the neural network utilized three sets of data and predict the corresponding output objective. The acceptable range of input–output data is illustrated in Figure 4. Each NN is constructed on a specific topology. Here, the topology is defined as the structure of the network. As can be seen in Figure 4, the utilized neural network is formed of three layers in order to estimate the target output, i.e. the viscosity of SiO<sub>2</sub> /ethylene glycol–water nanofluid.

A series of weighted coefficients are used to link input and output. (2\*5)10 edges are placed between the first layer and the second layer. Five (1\*5) edges are placed between the second and third layers. A weight is assigned to each edge. The weights of these edges are presented as a  $[IW]_{2 \times 5}$  matrix and a  $[LW]_{5 \times 1}$  matrix, respectively. The output is yielded from input data as follows:

$$\mu = [LW]_{1 \times 5} \times \tan h \left( [IW]_{5 \times 2} \times \begin{bmatrix} \dot{d} \\ phi \\ T \end{bmatrix}_{3 \times 1} + [b_1]_{5 \times 1} \right) + [b_2]_{1 \times 1}. \quad (6)$$

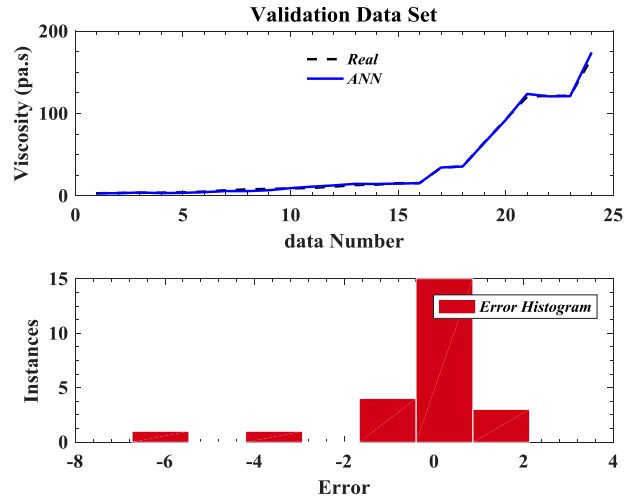


**Figure 5.** Modeled versus experimentally measured data – validation step (24 data).

Based on Equation (6), the output objective of the neural network is simply calculated through a mathematical formulation. The elements of  $[IW]_{5 \times 2}$ ,  $[LW]_{1 \times 5}$ ,  $[b_1]_{5 \times 1}$ ,  $[b_2]_{1 \times 1}$  matrices are not known and are randomly assigned in the first iteration. During the training process, the elements of these matrices are manipulated in such a way that the output of the output ( $\mu_{NN}$ ) coincides with the real measured output ( $\mu_{real}$ ) and decreases the calculation error.

Model data error (in %) for three sets of training, testing, and validating is illustrated in Figures 6–7. The calculated modeling error of the training, validating, and testing steps are obtained as less than 0.5%, 0.6%, and 1%, respectively. The modeling error of the test stage is naturally more than modeling errors of train and validation steps since test data is not involved in the training step.

In Figure 8, the horizontal axis represents the actual viscosity and the vertical axis is the amount of viscosity yielded from the modeling procedure. Ideally, when the model is completely accurate, all points are located on the bisector of the 1st quadrant. The process is not ideal in practice. Therefore, due to inaccuracies some points scattered around the bisector line. The best passing line

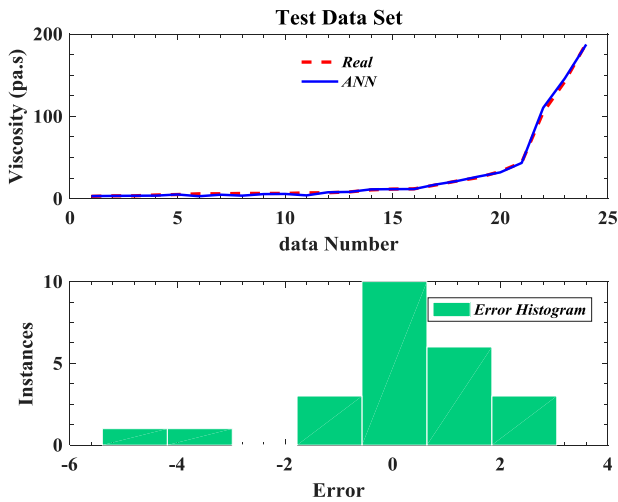


Figure 6. Modeled versus experimentally measured data – test step (24 data).

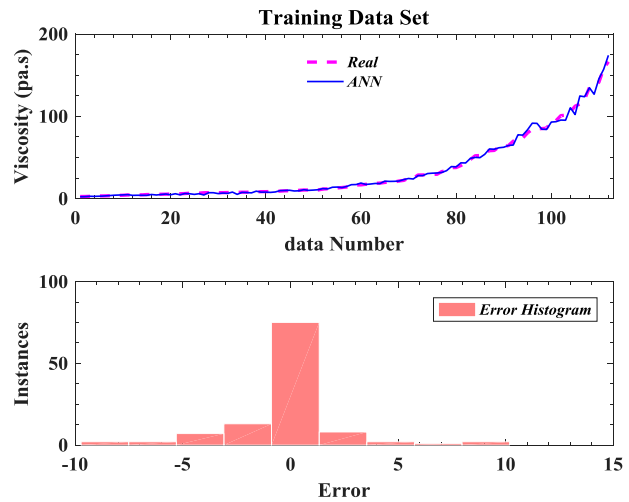


Figure 7. Modeled versus experimentally measured data – training step (112 data).

(MSE) and the correlation coefficient for all sets including training, validation, test, and total modeling process are illustrated in Figures 9 and 10.

In this section, a comparison was made between the results obtained from the NN modeling with the measurements. The total number of data used in the modeling procedure is 160, 112 for training, 24 for monitoring, and the rest for testing the network, as illustrated in the following, Figure 11.

The modeling error of the neural network is illustrated in Figure 12. The difference between the model’s response with the actual measurements is defined as the modeling error. The histogram diagram of the error is demonstrated in Figure 12. The histogram diagram of the error is calculated by dividing the total error interval into 20 equal segments and after that obtaining associated frequency of each interval and finally form the sets of training, validation, and testing. In fact, the frequency of

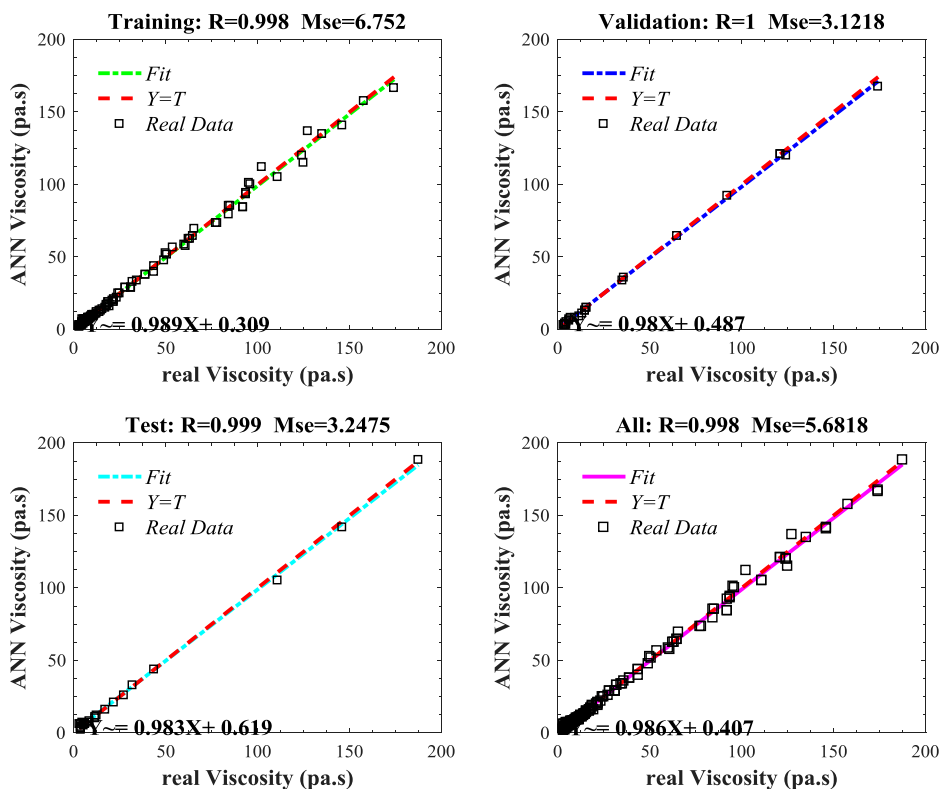
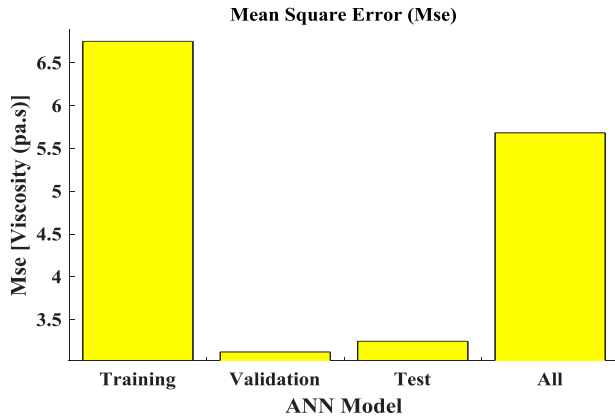
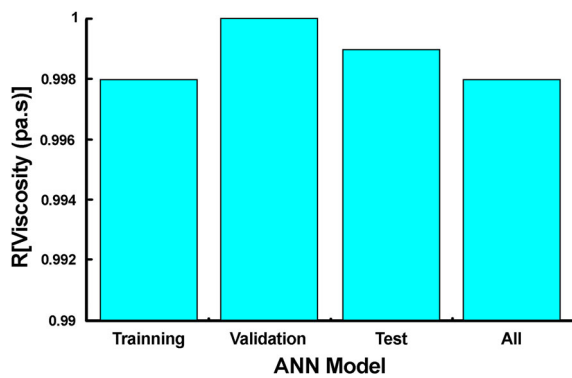


Figure 8. The regression line for training, validation, and test datasets.



**Figure 9.** Mean Square Error (MSE) for training, validation, test, and in total.



**Figure 10.** The correlation coefficient of training, validation, test, and in total.

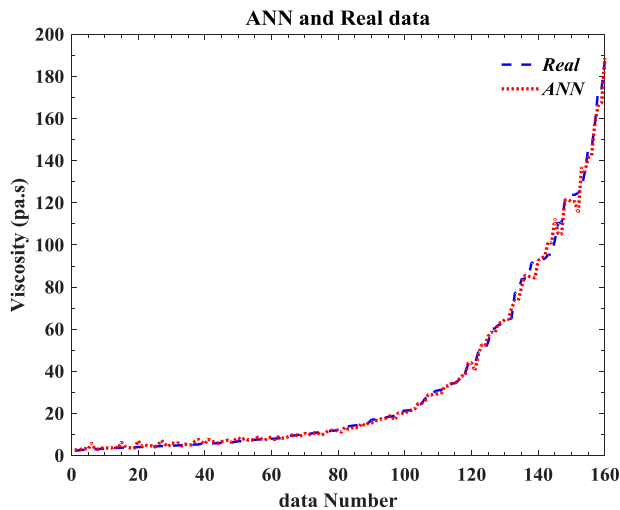


**Figure 11.** Comparison between the obtained results from the model with the actual measurements.

model prediction error in each sub-interval is presented in Figure 12.

Control of the MSE is considered as the stopping point for the training stage. Therefore, MSE curve is drawn by

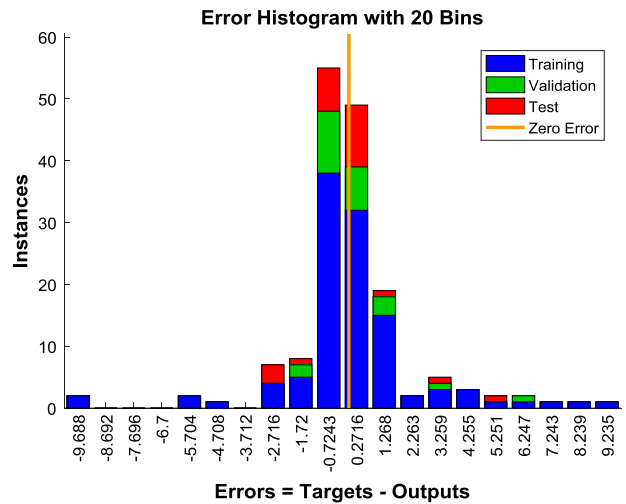


**Figure 12.** Histogram diagram of the error and the error frequency in each sub-interval.

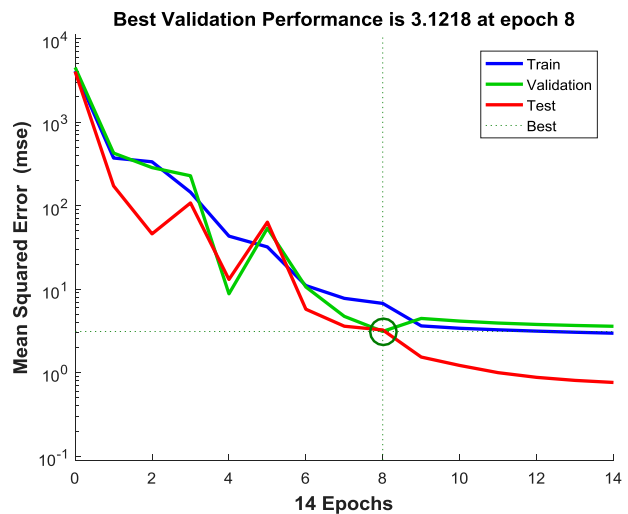


**Figure 13.** Mean Square error diagram in different iterations of the training stage of the viscosity estimating process.

considering the number of iterations of the training stage (Figure 13). Monitoring MSE for test and validation data is performed similar to the training data in various iterations, and when the validation data error starts to rise, the training phase should be ended. Iteration number 8 is the point which the most generalization occurs. In order to enhance the generalization trend and to lower overfitting, the training process is set to be stopped when the validation error reaches its minimum value. Furthermore, the mean square error (MSE) in every stage, i.e. training, validation, and test, is analyzed and demonstrated that the MSE results are approximately equal. Therefore, it can be seen that the overfitting issue does not happen.

The error fluctuation of the training stage is illustrated in Figure 14. The value of MSE is progressively

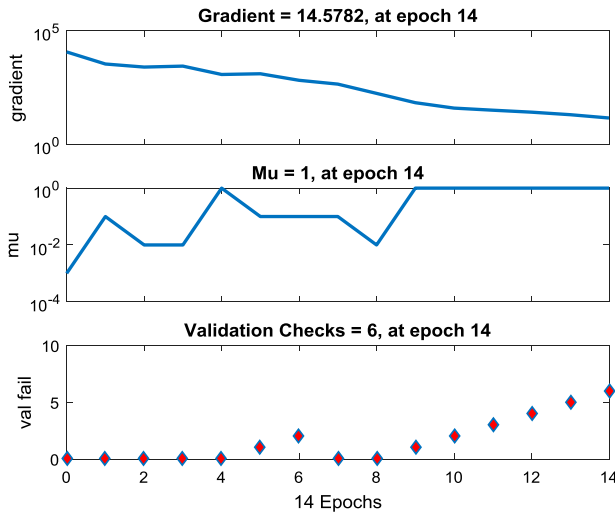


**Figure 14.** Error fluctuation during the training stage.

calculated in each iteration for the validation data. The stopping point of the training stage is when the validation error starts to reduce. The value of the validation error is not reducing in six iterations, therefore, the algorithm should be continued. The number 6, validation check, is defined as the stop training index and can be easily adjusted in the software. The output response of the model is extracted when the validation error reaches its lowest value. In Figure 14, from 8th to 14th iterations (6 consecutive iterations), the validation error has an augmenting development. Therefore, the training algorithm is terminated and the eighth iteration is reported as the output. The mean square error is calculated as follows:

$$\text{MSE} = \sum_{i=1}^n \frac{(\mu_{\text{NN}} - \mu_{\text{Real}})^2}{Ne}, \quad (7)$$

where  $\mu_{\text{NN}}$  and  $\mu_{\text{Real}}$  are the obtained value of the nanofluid's viscosity from the neural network model and the measured value from the experiments, respectively.  $Ne$  represents the total number of samples.

In Figure 15, the horizontal axis expresses the difference between the actual and estimated viscosity of the nanofluid and the vertical axis demonstrates the error rate obtained from the modeling. A meaningful relationship can be seen and illustrates that the predicting process has been successfully performed. To make a comparison between the presented model and other works which were previously published in the literature, i.e. the FCM-ANFIS model (Mehrabi, Sharifpur, & Meyer, 2013), Mean relative error of the results were calculated and a comparison was made (Table 1). Based on the comparison, the MRE of both intelligent techniques is in the same vicinity and the employed model of this study has a smaller

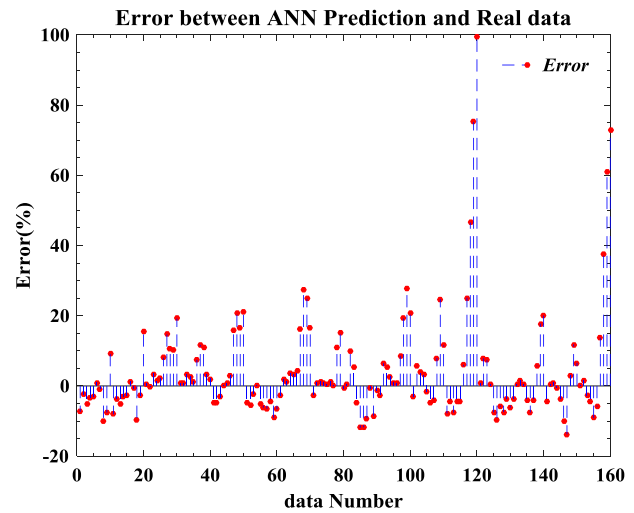


**Figure 15.** Range of error between estimated and real data.

**Table 1.** MRE comparison of the FCM-ANFIS model and the applied MLP-RBF model of this study.

	FCM-ANFIS	This study
Mean relative error (MRE)	11%	9.7%

MRE in comparison to the FCM-ANFIS model.

$$\text{MRE} = \sum_{i=1}^n 100 \times \frac{|\mu_{\text{NN}} - \mu_{\text{Real}}|}{Ne}. \quad (8)$$

#### 4. Conclusion

In order to demonstrate the significant role of intelligent methods in engineering mediums, dynamic viscosity of SiO<sub>2</sub>-water-ethylene glycol nanofluid was studied by the ANN approach. In this investigation, 160 experimentally measured data were collected from the literature. ANN approach is employed to model the effect of adding SiO<sub>2</sub> on the dynamic viscosity of the ethylene glycol-water fluid to be used in further investigations of fluid dynamic or heat transfer researches. MLP-RBF estimation algorithm is selected and their outputs are assessed through error analysis. It was obtained from the results that the model demonstrated acceptable output which was so close to the actual measurements. Error analysis illustrated that the implemented method was able to model the dynamic viscosity with high accuracy since the MSE and the correlation coefficient were obtained 5.5 and 0.998 Pa s, respectively. It can be highlighted that the accuracy of the model can be enhanced by providing a more complete dataset. Therefore, it is highly recommended to collect more real data through experiments to demonstrate and to approve the validity of the model.

## Acknowledgment

The authors would like to thank Miss. Samira Ghafourian for her kind help to enhance the worth of this work.

## Disclosure statement

No potential conflict of interest was reported by the authors.

## References

- Abdolbaqi, M. K., Sidik, N. A. C., Rahim, M. F. A., Mamat, R., Azmi, W. H., Yazid, M. N. A. W. M., & Najafi, G. (2016). Experimental investigation and development of new correlation for thermal conductivity and viscosity of Bio-Glycol/water based SiO<sub>2</sub> nanofluids. *International Communications in Heat and Mass Transfer*, 77, 54–63. <https://doi.org/10.1016/J.ICHEATMASSTRANSFER.2016.07.001>.
- Ahmadi, M. A. (2015). Developing a robust surrogate model of chemical flooding based on the artificial neural network for enhanced oil recovery implications. *Mathematical Problems in Engineering*, 2015. <https://doi.org/10.1155/2015/706897>.
- Ahmadi, M. A., & Mahmoudi, B. (2016). Development of robust model to estimate gas–oil interfacial tension using least square support vector machine: Experimental and modeling study. *The Journal of Supercritical Fluids*, 107, 122–128. <https://doi.org/10.1016/J.SUPFLU.2015.08.012>.
- Ahmadi, M. H., Mohseni-Gharyehsafa, B., Farzaneh-Gord, M., Jilte, R. D., Kumar, R., & Wing, C. K. (2019). Applicability of connectionist methods to predict dynamic viscosity of silver/water nanofluid by using ANN-MLP, MARS and MPR algorithms. *Engineering Applications of Computational Fluid Mechanics*, 13(1), 220–228. <https://doi.org/10.1080/19942060.2019.1571442>.
- Ahmadi, M. H., Sadeghzadeh, M., Raffiee, A. H., & Chau, K. (2019). Applying GMDH neural network to estimate the thermal resistance and thermal conductivity of pulsating heat pipes. *Engineering Applications of Computational Fluid Mechanics*, 13(1), 327–336. <https://doi.org/10.1080/19942060.2019.1582109>.
- Ahmadi, M. H., Tatar, A., Seifaddini, P., Ghazvini, M., Ghasempour, R., & Sheremet, M. A. (2018). Thermal conductivity and dynamic viscosity modeling of Fe<sub>2</sub>O<sub>3</sub>/water nanofluid by applying various connectionist approaches. *Numerical Heat Transfer, Part A: Applications*, 74(6), 1301–1322. <https://doi.org/10.1080/10407782.2018.1505092>.
- Alawi, O. A., Sidik, N. A. C., Xian, H. W., Kean, T. H., & Kazi, S. N. (2018). Thermal conductivity and viscosity models of metallic oxides nanofluids. *International Journal of Heat and Mass Transfer*, 116, 1314–1325. <https://doi.org/10.1016/J.IJHEATMASSTRANSFER.2017.09.133>.
- Amani, M., Amani, P., Jumholkul, C., Mahian, O., & Wongwises, S. (2018). Hydrothermal optimization of SiO<sub>2</sub>/water nanofluids based on attitudes in decision making. *International Communications in Heat and Mass Transfer*, 90, 67–72. <https://doi.org/10.1016/J.ICHEATMASSTRANSFER.2017.10.008>.
- Azari, A., Kalbasi, M., Derakhshandeh, M., & Rahimi, M. (2013). An experimental study on nanofluids convective heat transfer through a straight tube under constant heat flux. *Chinese Journal of Chemical Engineering*, 21(10), 1082–1088. [https://doi.org/10.1016/S1004-9541\(13\)60618-7](https://doi.org/10.1016/S1004-9541(13)60618-7).
- Azmi, W. H., Sharma, K. V., Sarma, P. K., Mamat, R., Anuar, S., & Dharma Rao, V. (2013). Experimental determination of turbulent forced convection heat transfer and friction factor with SiO<sub>2</sub> nanofluid. *Experimental Thermal and Fluid Science*, 51, 103–111. <https://doi.org/10.1016/J.EXPTHERMFLUSCI.2013.07.006>.
- Baghban, A., Sasanipour, J., Pourfayaz, F., Ahmadi, M. H., Kasaean, A., Chamkha, A. J., . . . Chau, K. (2019). Towards experimental and modeling study of heat transfer performance of water–SiO<sub>2</sub> nanofluid in quadrangular cross-section channels. *Engineering Applications of Computational Fluid Mechanics*, 13(1), 453–469. <https://doi.org/10.1080/19942060.2019.1599428>.
- Bobbo, S., Colla, L., Scattolini, M., Agresti, F., Barison, S., Pagura, C., . . . Uniti, C. S. (2011). Thermal conductivity and viscosity measurements of water-based silica nanofluids. *Consiglio Nazionale Delle Ricerche*, 2, 478–481.
- Cardellini, A., Fasano, M., Bozorg Bigdeli, M., Chiavazzo, E., & Asinari, P. (2016). Thermal transport phenomena in nanoparticle suspensions. *Journal of Physics Condensed Matter*, 28, 48. <https://doi.org/10.1088/0953-8984/28/48/483003>.
- Chau, K. (2017). *Use of Meta-Heuristic Techniques in Modelling*. Chuntian, C., & Chau, K. W. (2002). Three-person multi-objective conflict decision in reservoir flood control. *European Journal of Operational Research*, 142(3), 625–631. [https://doi.org/10.1016/S0377-2217\(01\)00319-8](https://doi.org/10.1016/S0377-2217(01)00319-8).
- Dalkılıç, A. S., Açıkgöz, Ö, Küçükıldırım, B. O., Eker, A. A., Lüleci, B., Jumholkul, C., & Wongwises, S. (2018). Experimental investigation on the viscosity characteristics of water based SiO<sub>2</sub>-graphite hybrid nanofluids. *International Communications in Heat and Mass Transfer*, 97, 30–38. <https://doi.org/10.1016/J.ICHEATMASSTRANSFER.2018.07.007>.
- Du, K., & Swamy, M. (2006). *Neural networks in a soft computing framework*. London: Springer-Verlag.
- Escher, W., Brunswiler, T., Shalkevich, N., Shalkevich, A., Burgi, T., Michel, B., & Poulikakos, D. (2011). On the cooling of electronics with nanofluids. *Journal of Heat Transfer*, 133(5), 51401–51411. <http://dx.doi.org/10.1115/1.4003283>
- Fotovatikhah, F., Herrera, M., Shamshirband, S., Chau, K., Ardabili, S. F., & Piran, M. J. (2018). Survey of computational intelligence as basis to big flood management: Challenges, research directions and future work. *Engineering Applications of Computational Fluid Mechanics*, 12(1), 411–437. <https://doi.org/10.1080/19942060.2018.1448896>.
- Ghalandari, M., Mirzadeh Koohshahi, E., Mohamadian, F., Shamshirband, S., & Chau, K. W. (2019). Numerical simulation of nanofluid flow inside a root canal. *Engineering Applications of Computational Fluid Mechanics*, 13(1), 254–264. <https://doi.org/10.1080/19942060.2019.1578696>.
- Ghasemi, S., & Karimipour, A. (2018). Experimental investigation of the effects of temperature and mass fraction on the dynamic viscosity of CuO–paraffin nanofluid. *Applied Thermal Engineering*, 128, 189–197. <https://doi.org/10.1016/J.APPLTHERMALENG.2017.09.021>.
- Goh, A. T. C. (1995). Back-propagation neural networks for modeling complex systems. *Artificial Intelligence in Engineering*, 9(3), 143–151. [https://doi.org/10.1016/0954-1810\(94\)00011-S](https://doi.org/10.1016/0954-1810(94)00011-S).
- Gupta, M., Singh, V., Kumar, R., & Said, Z. (2017). A review on thermophysical properties of nanofluids and heat transfer

- applications. *Renewable and Sustainable Energy Reviews*, 74, 638–670. <https://doi.org/10.1016/J.RSER.2017.02.073>.
- Hajikhodaverdikhan, P., Nazari, M., Mohsenizadeh, M., Shamshirband, S., & Chau, K. W. (2018). Earthquake prediction with meteorological data by particle filter-based support vector regression. *Engineering Applications of Computational Fluid Mechanics*, 12(1), 679–688. <https://doi.org/10.1080/19942060.2018.1512010>.
- Hamid, K. A., Azmi, W. H., Nabil, M. F., Mamat, R., & Sharma, K. V. (2018). Experimental investigation of thermal conductivity and dynamic viscosity on nanoparticle mixture ratios of TiO<sub>2</sub>–SiO<sub>2</sub> nanofluids. *International Journal of Heat and Mass Transfer*, 116, 1143–1152. <https://doi.org/10.1016/J.IJHEATMASSTRANSFER.2017.09.087>.
- Kahani, M., Ahmadi, M. H., Tatar, A., & Sadeghzadeh, M. (2018). Development of multilayer perceptron artificial neural network (MLP-ANN) and least square support vector machine (LSSVM) models to predict Nusselt number and pressure drop of TiO<sub>2</sub>/water nanofluid flows through non-straight pathways. *Numerical Heat Transfer, Part A: Applications*, 0(0), 1–17. <https://doi.org/10.1080/10407782.2018.1523597>.
- Kulkarni, D. P., Namburu, P. K., Bargar, H. E., & Das, D. K. (2008). Convective heat transfer and fluid dynamic characteristics of SiO<sub>2</sub> ethylene glycol/water nanofluid. *Heat Transfer Engineering*, 29(12), 1027–1035. <https://doi.org/10.1080/01457630802243055>.
- Maddah, H., Aghayari, R., Mirzaee, M., Ahmadi, M. H., Sadeghzadeh, M., & Chamkha, A. J. (2018). Factorial experimental design for the thermal performance of a double pipe heat exchanger using Al<sub>2</sub>O<sub>3</sub>-TiO<sub>2</sub> hybrid nanofluid. *International Communications in Heat and Mass Transfer*, 97, 92–102. <https://doi.org/10.1016/j.icheatmasstransfer.2018.07.002>.
- Mahyari, A. A., Karimipour, A., & Afrand, M. (2019). Effects of dispersed added graphene oxide–silicon carbide nanoparticles to present a statistical formulation for the mixture thermal properties. *Physica A: Statistical Mechanics and Its Applications*, 521, 98–112. <https://doi.org/10.1016/J.PHYSA.2019.01.035>.
- Mehrabi, M., Sharifpur, M., & Meyer, J. P. (2013). Viscosity of nanofluids based on an artificial intelligence model. *International Communications in Heat and Mass Transfer*, <https://doi.org/10.1016/j.icheatmasstransfer.2013.02.008>.
- Moldoveanu, G. M., Huminic, G., Minea, A. A., & Huminic, A. (2018). Experimental study on thermal conductivity of stabilized Al<sub>2</sub>O<sub>3</sub> and SiO<sub>2</sub> nanofluids and their hybrid. *International Journal of Heat and Mass Transfer*, 127, 450–457. <https://doi.org/10.1016/j.ijheatmasstransfer.2018.07.024>.
- Namburu, P. K., Kulkarni, D. P., Dandekar, A., & Das, D. K. (2007). Experimental investigation of viscosity and specific heat of silicon dioxide nanofluids. *Micro & Nano Letters*, 2(3), 67–71. <https://doi.org/10.1049/mnl:20070037>.
- Nazari, M. A., Ahmadi, M. H., Sadeghzadeh, M., Shafii, M. B., & Goodarzi, M. (2019). A review on application of nanofluid in various types of heat pipes. *Journal of Central South University*, 26(5), 1021–1041. <https://doi.org/10.1007/s11771-019-4068-9>.
- Peñas, J. R. V., de Zárate, J. M., & Khayet, M. (2008). Measurement of the thermal conductivity of nanofluids by the multicurrent hot-wire method. *Journal of Applied Physics*, 104(4), 44314. <https://doi.org/10.1063/1.2970086>.
- Ramezanizadeh, M., Ahmadi, M. A., Ahmadi, M. H., & Alhuyi Nazari, M. (2019). Rigorous smart model for predicting dynamic viscosity of Al<sub>2</sub>O<sub>3</sub>/water nanofluid. *Journal of Thermal Analysis and Calorimetry*, 137(1), 307–316. <https://doi.org/10.1007/s10973-018-7916-1>.
- Ramezanizadeh, M., Alhuyi Nazari, M., Ahmadi, M. H., & Açikkalp, E. (2018). Application of nanofluids in thermosyphons: A review. *Journal of Molecular Liquids*, 272, 395–402. <https://doi.org/10.1016/J.MOLLIQ.2018.09.101>.
- Ramezanizadeh, M., Alhuyi Nazari, M., Ahmadi, M. H., & Chau, K. (2019). Experimental and numerical analysis of a nanofluidic thermosyphon heat exchanger. *Engineering Applications of Computational Fluid Mechanics*, 13(1), 40–47. <https://doi.org/10.1080/19942060.2018.1518272>.
- Ramezanizadeh, M., Alhuyi Nazari, M., Ahmadi, M. H., Lorenzini, G., & Pop, I. (2019). A review on the applications of intelligence methods in predicting thermal conductivity of nanofluids. *Journal of Thermal Analysis and Calorimetry*, <https://doi.org/10.1007/s10973-019-08154-3>.
- Razavi, R., Sabaghmoghadam, A., Bemani, A., Baghban, A., Chau, K., & Salwana, E. (2019). Application of ANFIS and LSSVM strategies for estimating thermal conductivity enhancement of metal and metal oxide based nanofluids. *Engineering Applications of Computational Fluid Mechanics*, 13(1), 560–578. <https://doi.org/10.1080/19942060.2019.1620130>.
- Sadeghzadeh, M., Ahmadi, M. H., Kahani, M., Sakhaeinia, H., Chaji, H., & Chen, L. (2019). Smart modeling by using artificial intelligent techniques on thermal performance of flat-plate solar collector using nanofluid. *Energy Science & Engineering*. <https://doi.org/10.1002/ese3.381>.
- Sahoo, B. C., Das, D. K., Vajjha, R. S., & Satti, J. R. (2013). Measurement of the thermal conductivity of silicon dioxide nanofluid and development of correlations. *Journal of Nanotechnology in Engineering and Medicine*, 3(4), 41006–41010. <http://dx.doi.org/10.1115/1.4024003>.
- Sepehr, M., Baghban, M., Ghanbari, A., Bozorgvar, M. E., & Baghban, A. (2018). Modeling dynamic viscosity of n-alkanes using LSSVM technique. *Energy Sources, Part A: Recovery, Utilization and Environmental Effects*, 40(16), 1966–1973. <https://doi.org/10.1080/15567036.2018.1486906>.
- Taherei Ghazvinei, P., Darvishi, H. H., Mosavi, A., Bin Wan Yusof, K., Alizamir, M., Shamshirband, S., & Chau, K. W. (2018). Sugarcane growth prediction based on meteorological parameters using extreme learning machine and artificial neural network. *Engineering Applications of Computational Fluid Mechanics*, 12(1), 738–749. <https://doi.org/10.1080/19942060.2018.1526119>.
- Talib, S. F. A., Azmi, W. H., Zakaria, I., Mohamed, W., Mamat, A. M. I., Ismail, H., & Daud, W. R. W. (2015). Thermophysical properties of silicon dioxide (SiO<sub>2</sub>) in ethylene glycol/water mixture for proton exchange membrane fuel cell cooling application. *Energy Procedia*, 79, 366–371. <https://doi.org/10.1016/J.EGYPRO.2015.11.504>.
- Wu, C. L., & Chau, K. W. (2011). Rainfall-runoff modeling using artificial neural network coupled with singular spectrum analysis. *Journal of Hydrology*, 399(3–4), 394–409. <https://doi.org/10.1016/j.jhydrol.2011.01.017>.
- Zendehboudi, A., & Li, X. (2017). Robust predictive models for estimating frost deposition on horizontal and parallel

- surfaces. *International Journal of Refrigeration*, 80, 225–237. <https://doi.org/10.1016/J.IJREFRIG.2017.05.013>.
- Zendehboudi, A., & Tatar, A. (2017). Utilization of the RBF network to model the nucleate pool boiling heat transfer properties of refrigerant-oil mixtures with nanoparticles. *Journal of Molecular Liquids*, 247, 304–312. <https://doi.org/10.1016/J.MOLLIQ.2017.09.105>.
- Zendehboudi, A., Wang, B., & Li, X. (2017). Robust model to predict the migration ratios of nanoparticles during the pool-boiling process of nanorefrigerants. *International Communications in Heat and Mass Transfer*, 84, 75–85. <https://doi.org/10.1016/J.ICHEATMASSTRANSFER.2017.03.012>.
- Zhao, N., Wen, X., Yang, J., Li, S., & Wang, Z. (2015). Modeling and prediction of viscosity of water-based nanofluids by radial basis function neural networks. *Powder Technology*, 281, 173–183. <https://doi.org/10.1016/j.powtec.2015.04.058>.

## Appendix

**Table A1.** Weights and biases of the MLP neural networks.

Neuron	Hidden layer				Output layer	
	Weight		Biases		Weight	Bias
	$\varphi$	Size	$T$	$b_j$		$b_k$
1	0.78845	12.7723	−3.954	7.5468	2.2986	1.0966
2	0.28628	−4.4808	0.76853	−1.6808	2.0457	
3	0.091406	17.0011	1.0539	3.877	−2.0247	
4	2.2719	−8.2645	−4.9167	−9.7804	0.41152	
5	18.2464	−0.06705	9.6483	−15.7871	−0.07045	
6	−0.038527	−0.17537	1.2785	1.7151	−2.5001	
7	−0.82137	−7.9087	5.2944	4.8629	−1.9015	